BNL 50866

REGENERATIVE PROCESS FOR DESULFURIZATION OF HIGH TEMPERATURE COMBUSTION AND FUEL GASES

QUARTERLY PROGRESS REPORT NO. 8
JANUARY 1-MARCH 31, 1978

PROCESS SCIENCES DIVISION
DEPARTMENT OF ENERGY AND ENVIRONMENT

BROOKHAVEN NATIONAL LABORATORY
ASSOCIATED UNIVERSITIES, INC.

UNDER CONTRACT NO. EY-76-C-02-0016 WITH THE
UNITED STATES DEPARTMENT OF ENERGY

DISCLAIMER

BNL 50866
UC-90e
(Coal Conversion and Utilization—
Direct Combustion of Coal - TID-4500)

REGENERATIVE PROCESS FOR DESULFURIZATION OF HIGH TEMPERATURE COMBUSTION AND FUEL GASES

QUARTERLY PROGRESS REPORT NO. 8
JANUARY 1-MARCH 31, 1978

Contributors:

R.T. Yang
A.S. Albanese
J.M. Chen
G. Farber
F.B. Kainz
J. Pruzansky
M-S. Shen
C.L. Steen
M. Steinberg

M. Steinberg, Head
R.T. Yang, Project Leader

PROCESS SCIENCES DIVISION
DEPARTMENT OF ENERGY AND ENVIRONMENT

BROOKHAVEN NATIONAL LABORATORY
UPTON, NEW YORK 11973

NOTICE

Printed in the United States of America
Available from
National Technical Information Service
U.S. Department of Commerce
5285 Port Royal Road
Springfield, VA 22161
Price: Printed Copy $5.25; Microfiche $3.00

July 1978 380 copies

Table of Contents

Abstract

A highly reactive β-dicalcium silicate powder sample has been acquired from Professor D. Roy of Pennsylvania State University. The sample was prepared by the Roy Evaporative Decomposition of Solution (EDS) process. We will use it in conjunction with our ash-binder pelletizing technique to form a highly regenerable and reactive sorbent for fluidized bed combustion. Other techniques of forming reactive silicates are also being studied.

Simplified mathematical models have been developed for kiln regeneration based on the data with a small quartz rotary kiln reactor. The model provides better understanding for scale-up of the promising Brookhaven Kiln Regeneration Process.

The Fe_2O_3 catalyzed sulfation and regeneration process has been further studied with a small quartz fluidized-bed sulfator and a small rotary kiln regenerator. Ten sulfation-regeneration cycles will be completed within the next reporting quarter. After completion of the cyclic experiments, we will make recommendations for field testing, i.e., testing in one of the DOE pilot fluidized bed combustors and regenerators.

The reactivity of a reconstructed $CaSO_4$ is indeed higher than the original sample. The reconstructed sample was maed via the procedure: $CaSO_4 \xrightarrow{red.} CaS \xrightarrow{oxid.} CaSO_4$. We plan to further understand the morphological and structural changes taking place in the process.

A detailed analysis and a review of the high temperature $CaSO_4$ regeneration mechanism were made. All possible reactions in the system

were taken into account. Rates of the more important (rapid) ones were measured. Existence of a gaseous intermediate indeed was acertained and some mechanisms were proposed. Understanding of the mechanism will be useful in improving all the regeneration processes being developed.

Kinetics of the rapid reaction between CaO and SO_3 are being studied and the work will be completed shortly. This is part of our effort to understand the mechanism both in sulfation and regeneration.

A good attempt has been made to use ZnO as a regenerable sorbent for hot fuel gas desulfurization. The evaporation rate of the sorbent in a reducing atmosphere is too high for this sorbent to be of practical use.

Regenerative Process for Desulfurization of High Temperature Combustion and Fuel Gases

Quarterly Progress Report No. 8
January 1-March 31, 1978

A. Calcium Silicates and Silica-Based Materials as Regenerable Sorbents (Yang, Shen, Steinberg)

As reported in the previous reports of this program, we have found that sulfated calcium silicates are more regenerable than sulfated limestone. For example, the sulfation rate under FBC conditions of a commercial silicate insulation material supplied by Fibreboard Corporation was about the same as Greer limestone. The material contained primarily $CaSiO_3$. More important, the regeneration rate was about seven times higher. We have been searching for methods of preparing reactive calcium silicates.

During the last quarter, Professor Della Roy from Pennsylvania State University consulted with us on this subject. She has developed a process for preparing a highly reactive β-calcium silicate. The method is described in a paper which will be published soon in Il Cemento. It involved spraying a solution of calcium nitrate and Ludox (duPont trade name for a Colloidal SiO_2) in a hot zone about 1000°C. A highly reactive β-Ca_2SiO_4 is formed rapidly. Unfortunately, the size of the silicate is very fine (∿ 1μm). We plan to use it, combined with our coal ash binding technique we are developing for FBC. The powder will be pelletized with fine coal ash. Sulfation and regeneration rates will be measured. If successful, this process should be the best regenerable sorbent yet developed.

We also plan to strengthen our silicate program in the coming quarters. Professor Roy, as well as our own staff members, will be devoting more time and efforts in searching for techniques to form the reactive silicates. In this report, both dry and wet processes are being studied. The wet processes will be similar to the Roy or the EDS (Evaporative Decomposition of Solutions) process.

As proposed in the last quarterly report, we are investigating a new class of synthetic regenerable sorbent which involves calcium oxide supported on silica. In a typical experiment, high surface area porous silica gels (surface area 720-760 m^2/gram, pore volume 0.43 cc/gram) with 16/20 Tyler mesh size were immersed in a concentrated aqueous solution of calcium acetate and subsequently heat treated at 1000^{o}C (chosen ad the regeneration temperature) for four hours. The calcium loading was then analyzed. X-ray diffraction analysis showed that CaO was the predominant product. Trace amount of β-dicalcium silicate was detected. However, at the steady state in a continuous cyclic process, the contents of the silicates would increase with the number of cycles.

Our preliminary results showed that the sulfation rate was higher than the natural lime and that the sulfated sample is more regenerable than the sulfated lime. Experiments in progress are designed to study the effect of calcium loading on the sulfation rate and the related porosity, cyclic sorbent life study and attrition resistance.

B. Development of Brookhaven Kiln Regeneration Process (J. M. Chen, G. Farber, and R. T. Yang)

Previous investigation (BNL report 7) showed that the process of using a rotary kiln to regenerate sulfated lime with fly ash as the reductant could generate an SO_2-rich gas at 1000°C and also retain high reactivities of the regenerated materials. In this report, mathematical expressions for the unsteady state, semibatch reactor used for such process have been derived. This analysis was performed to gain more understanding while we are designing and constructing a larger scale kiln regenerator.

Regeneration experiments at 1000°C for various flow rates have been constructed. Results of these experiments have been correlated with the derived expressions. At low flow rates, when mass transfer resistances were predominant, the SO_2 concentration profile deviates from the analytical expressions. However, at high enough flow rates, the SO_2 concentration profiles could be well correlated by the mathematical descriptions. Using the mathematical expression rate constants can be extracted from the exit SO_2 concentration profiles.

A larger scale rotary kiln regenerator is currently under construction. The reactor will be made of quartz and will be completed in the next quarter. Experiments will be conducted to investigate the effects of particle size, various kinds of reductants, extent of sulfated material on reaction kinetics and to obtain the necessary data for design of rotary kiln regeneration process. A minikiln regenerator is being designed and procurement for the necessary parts are being assembled. Our goal is to obtain realistic process information necessary for

scale-up of the promising Brookhaven kiln regeneration process. The minikiln will be about 3-in. in diameter, 3-ft long, and with refractory lining. Heat for the process will be internally supplied by combustion of carbon. Because of inherent difficulties, we try to avoid sealing of the rotary parts by designing a magnetically driven kiln which is housed in a stationary "kiln" to accomplish this.

(2) Model Studies: Rotary Kiln Regeneration Process

(a) System Description and Assumptions

The reaction scheme considered in our laboratory to regenerate sulfated lime from FBC is

$$CaSO_4 + 2C \overset{r_1}{\rightarrow} CaS + 2CO_2$$

$$3CaSO_4 + CaS \overset{r_2}{\rightarrow} 4CaO + 4SO_2$$

using a rotary kiln as the regenerator. Here, the mathematical description for a horizontal kiln under unsteady state, isothermal and semibatch operational conditions is derived. Figure 1 illustrates the system.

The material balance for a differential increament of reactor is

Gas Phase:

Inert gas
$$\frac{\partial uC_1}{\partial z} + \frac{\partial C_1}{\partial t} = 0 \qquad (1)$$

CO_2
$$\frac{\partial uC_2}{\partial z} + \varepsilon \frac{\partial C_2}{\partial z} = k_{2m}A_2(C_{2s} - C_2) \qquad (2)$$

SO_2

$$\frac{\partial uC_3}{\partial z} + \varepsilon \frac{\partial C_3}{\partial t} = k_{3m}A_3(C_{3s}-C_3) \qquad (3)$$

Solid Phase:

$$-k_{2m}Al(C_{2s}-C_2) = \frac{(1-\varepsilon)}{b} \frac{\partial S_2}{\partial t} \qquad (4)$$

$$-k_{3m}Al(C_3s-C_3) = \frac{(1-\varepsilon)}{b_3} \frac{\partial S_3}{\partial t} \qquad (5)$$

where

C_i = gas concentration in bulk phase, (mole/c.c.)

z = distance of the reactor (cm)

ε = void fraction

k_{im} = mass transfer coefficient for i compound $\frac{1}{(\text{sec cm}^2)}$

a_i = surface area of the solid related to i compound reaction per unit volume of reactor $\frac{\text{cm}^2}{\text{cm}^3 \text{ reactor}}$

C_{is} = gas concentration of i compound on the solid surface $\frac{\text{mole}}{\text{c.c.}}$

u = superficial velocity (cm/sec)

S_i = solid molar concentration related to i compound reaction per unit volume of reactor $\frac{\text{mole}}{\text{cm}^3}$

b_i = stoichiometric coefficient for i compound reaction

t = time (sec)

i = gas compound, i=1 inert gas; i=2, CO_2; i=3, SO_2

T = temperature (^{o}k)

The solution of the above five equations with the following initial and boundary conditions

$t = 0 \quad S_i = S_{io}$ (initial solid concentration)

$z = 0 \quad C_1 = C_{10}, \; C_2 = C_3 = 0$

and with rate expressions for reactions 1, 2 will be able to describe the reactor performance.

It has been known that reaction 2 is the rate controlling step for the above two step regeneration process. Therefore, only reaction 2 will be considered in this derivation. Since the rate expression for this reaction was found to be in the first order with respect to solid ($CaSO_4$) concentration (Chapter E), to account also for SO_2 partial pressure effect on reaction rate. r_2 is written in the following form

$$\frac{\partial s}{\partial t} = -k\eta(Pe-P)S \qquad (6)$$

P and Pe are SO_2 partial pressure and equilibrium pressure respectively, and η is the effectiveness factor, which accounts for pore diffusion resistance.

The assumptions in this derivation are summarized in the following:

(1) No axial solid mixing but only radial mixing in the reactor.

(2) Gas velocity remains constant.

(3) Mass transfer resistance is negligible.

(4) Reaction rate r_1 is instantaneous with respect to r_2.

(5) Ideal gas behavior.

(6) Plug flow.

(b) Derivation

The differential equations required for consideration will then be

$$\frac{\partial s}{\partial t} = -k \cdot RT \cdot \eta (Ce - C) S \tag{7}$$

$$u \frac{\partial c}{\partial z} + \varepsilon_v \frac{\partial c}{\partial t} = \frac{(1-\varepsilon)}{b} \; k \cdot R \cdot T \cdot \eta (C_e - C) S \tag{8}$$

with

I. C. $t=0, \; S=So$

$z=0, \; C=0$

Before proceeding further, these questions will be put into dimensionless form by introducing the following reduced variables:

$$\xi = z \frac{kRT\eta C_e}{u}$$

$$\tau = \eta kRTC_e \left(t - \frac{z}{u} \varepsilon\right) \tag{9}$$

$$\overline{C} = \frac{c}{C_e} \qquad \beta = \frac{(1-\varepsilon)}{b} \; \frac{So}{C_e}$$

$$\overline{S} = \frac{S}{So}$$

Equations (7) and (8) become

$$\frac{\partial \overline{S}}{\partial \tau} = -(1-\overline{C})\overline{S} \tag{10}$$

$$\frac{\partial \overline{C}}{\partial \xi} = \frac{(1-\varepsilon)}{b} \cdot \frac{S_o}{C_e} (1-\overline{C})\overline{S} = \beta(1-\overline{C})\overline{S} \tag{11}$$

with

I. C. $\tau=0, \; \overline{S}=1$

$\xi=0, \; \overline{C}=0$

These equations can then be solved by method of characteristics. The solution is

$$\frac{C}{C_e} = \frac{e^{\beta\xi}-1}{e^{\beta\xi}+e^{\tau}-1} \tag{12}$$

$$\frac{S}{S_o} = \frac{e^{\beta\xi}}{e^{\beta\xi}+e^{\tau}-1} \tag{13}$$

(c) Analysis

Equations (12) and (13) show that the reactor performance depends on two groups of variables

$$\beta\xi = \frac{(1-\varepsilon)}{b} \cdot S_o \cdot z. \left(\frac{1}{u}\right) \eta kRT \tag{14}$$

and

$$\tau = \eta kRTC_e\left(t - \frac{z}{u}\varepsilon\right) \tag{15}$$

Figures 2 and 3 illustrate the effects of these variables on SO_2 and solid concentrations respectively. Increasing τ while fixing $\beta\xi$ reduces SO_2 concentration but increases the extent of regeneration, and increasing $\beta\xi$ while fixing τ can increase SO_2 concentration up to its equilibrium value for reaction 2. The magnitude of $\beta\xi$ can be enlarged by increasing solid loading, reactor length and reactivity and reducing superficial velocity, and the magnitude of τ depends primarily on reaction time.

The average solid concentration after a given time t is

$$S_{av} = S_o \int_0^z \frac{e^{\beta\xi}}{e^{\beta\xi}+e^{\tau}-1}\, dz \tag{16}$$

It $t >> \frac{z}{u} \cdot \varepsilon$, $\tau \approx$ constant, and equation (16) becomes

$$S_{av} = S_o \int_0^{\beta\xi} \frac{e^{\beta\xi}}{e^{\beta\xi}+e^{\tau}-1}\, d(\beta\xi) \cdot \frac{b \cdot u}{(1-\varepsilon) \cdot S_o \cdot \eta kRT}$$

and

$$\frac{S_{av}}{S_o} = \frac{bu}{(1-\varepsilon)S_o \eta kRT} \cdot \ln\left(\frac{e^{\beta\xi}+e^{\tau}-1}{e^{\tau}}\right)$$

The extent of regeneration is

$$1 - \frac{S_{av}}{S} = 1 - \frac{bu}{(1-\varepsilon)S_o \eta kRT} \ln\left(\frac{e^{\beta\xi}+e^{\tau}-1}{e^{\tau}}\right) \tag{17}$$

Since all the variables except η and k in equations (12)-(15) can be determined from experimental data, the product ηk can be calculated from measurements of the exit SO_2 concentration profile using the generalized curves in Figure 2b. However, an alternative approach for ηk determination can be obtained by rearranging equation (12) into:

$$\frac{C_e}{C} - 1 = \frac{e^{\tau}}{e^{\beta\xi}-1} \tag{18}$$

and

$$\ln\left(\frac{C_e}{C} - 1\right) = \eta kRTC_e t - \left[\eta kRTC_e \cdot \frac{\xi}{u} \varepsilon + \ln(e^{\beta\xi}-1)\right] \tag{19}$$

Therefore, the plot of $\ln\left(\frac{C_e}{C} - 1\right)$ versus time produces a straight line from whose slope ηk can be determined. These slopes for various flow rates will be the same provided that mass transfer effect is negligible. The intercepts, I's of the above plot, however, is effected by the flow rates; if $\beta\xi << 1$

$$I = \ln\left(\frac{C_e}{C} - 1\right)_{t=0} = -\eta kRTC_e \cdot \frac{\xi}{u} \varepsilon \tag{20}$$

and if $e^{\beta\xi} >> 1$

$$I = \ln\left(\frac{C_e}{C} - 1\right)_{t=0} = -\eta kRTz\left(\varepsilon C_3 + \frac{(1-\varepsilon)}{b} S_o\right) \cdot \frac{1}{u} \tag{21}$$

Hence, plots of intercept values versus $\frac{1}{u}$, in general, give linear relationship.

(d) Correlation With Experimental Results

To test the above mathematical analysis for reactor performance, experiments of using fly ash from FBC as the reductant to regenerate sulfated lime at 1000°C with various flow rates have been conducted. The experimental conditions were:

Reactor:

diameter: 25mm

length: 76 mm (which was the maximum length that could retain uniform temperature for the apparatus - apparatus was described in Report No. 6).

Sulfated Greer Lime:

composition: 32% Ca^{++}, 15% $SO_4^{=}$, 1.28% Fe^{+++}, 24% $CO_3^{=}$, 11.9% SiO_2

size: 16/20

weight: 2 grams

Fly Ash:

composition: 12.5% C, 5.24% S, 14.6% $SO_4^{=}$ and 7.24% $CO_3^{=}$

size: -200

weight: .202 grams ($\frac{C}{S}=\frac{1}{2}$)

carrier gas: Ar

temperature: 1000°C

running time: 1 hour

initial time: Defined as the time when the temperature reads 950°C

Typical exit CO_2 and SO_2 compositions with respect to time are given in Figure 4. At low gas velocities, the history of CO_2 interferred with SO_2 history for most of the reaction times, while at high velocities, very little interaction of CO_2 concentration profile with SO_2 concentration profile was observed. This indicates that assumption (4), $r_1 >> r_2$, is only valid at high gas velocities.

The measured SO_2 concentrations in the exit for the various flow rates were plotted in Figure 5. These profiles first increased with time, due to temperature rising and time lag in sampling, followed by decay in concentration. Except for those results obtained at low flow rates ($\leq$ 10 sccm), the shapes of decaying SO_2 concentration profiles were similar to the curves in Figure 2b. This is because at low gas flow rates mass transfer resistance became predominant. Also, because reaction (1) became competitive with reaction (2) at low flow rates, the unreacted carbon in the reactor could react with SO_2,

$$3C + 2SO_2 \rightarrow CO_2 + S_2 + 2CO$$

to reduce SO_2 concentration. Therefore, equilibrium SO_2 concentration could not be obtained merely by lowering the flow rates.

Using the decaying portion of the SO_2 concentration profiles, plots of $\log \left(\frac{C_e}{C} - 1\right)$ versus time (C_e=10% at 1000°C, 1 atm) were then made as shown in Figure 6. Straight lines could generally be obtained for SO_2 concentration larger than 0.1%. Except for low carrier gas flow rates ($\leq$ 10 sccm) about the same values of the slopes of these lines were found. Plotting the intercepts from Figure 6 against

reciprocal flow rates, as shown in Figure 7, also gave a linear relationship. From these results, it is apparent that the above mathematical expressions (equations (12) and (13)) can be used to describe the reactor performance.

The above experimental results indicate that values of $\beta\xi$ (c.f. Figure 2b) were too small to have equilibrium SO_2 concentration. To enlarge its magnitude without changing gas velocity and reaction temperatures, one can only increase the solid loading per unit volume and/or the length of the reactor. Since too much loading reduces solid-solid mixing, a larger size reactor is required to obtain higher exit SO_2 concentration. Currently a rotary quartz reactor with a 3 ft reaction zone is under construction and will be completed in the next quarter. With the new apparatus, a series of experiments will be conducted to investigate the reaction kinetics under the effects of reactant sizes, sources or reactants, extent of sulfation, etc., and to obtain the necessary data for future design of the rotary kiln regeneration process.

C. Iron Oxide Catalyzed Sulfation and Regeneration (R. T. Yang, M-S. Shen, and J. Pruzansky

(1) Introduction

For fluidized-bed combustion of coal, limestones are the principal bed materials being considered for the sorption of SO_2. However, the rate of SO_2 capture by the sorbent is rather low. The use of additives in a fluidized-bed coal combustion system to increase the SO_2-sorption capabilities of limestone has received considerable

attention. One of the processes being developed in this program is to utilize iron compounds for the enhancement of the SO_2 sorption of limestones. It has been shown that the iron oxide not only catalyzes the sulfation rate but also increases the capacity for SO_2 absorption.[1] It is therefore an objective of this study to provide a method for preparing limestone so as to improve its SO_2 removal properties in fluidized-bed combustion and increase the calcium utilization.

Iron oxides are also shown to accelerate the regeneration of the lime from the sulfate. Therefore, the limestones with impregnated iron oxide and carried over from the combustor increase the regeneration rate. On the other hand, if the regeneration of sulfated sorbents is not economical, this process also provides a method for once-through systems to reduce the lime requirement due to the improved SO_2 sorption by the lime.

(2) Experimental

(a) Sulfation System

Materials

The uncalcined Greer limestone (16/20 Tyler mesh) were dipped or soaked in $Fe_2(SO_4)_3$ aqueous solution of about 2 to 3 molar concentration at room temperature for 30 minutes. The treated samples were air-dried. The unused ferric sulfate powder was sieved out and dissolved in water to be reused for fresh limestone. The treated sample contained about 0.5 to 1.5 weight percent Fe_2O_3 (based on CaO) deposited on the uncalcined limestone. The iron contents were determined by atomic absorption techniques.

Apparatus and Procedure

For TGA studies, the apparatus used for the sulfation rate measurements was the duPont thermo-analyzer Model 951. A small quartz boat with an area of about 0.6 cm^2 was used as the sample holder. A quartz tube packed with alumina chips and housed in a tubular furnace served as the preheater for the reactant gases. About 40 mg of uncalcined Greer limestone sample (16/20 Tyler mesh) was spread in a thin layer on the holder as the solid reactant. The samples were calcined and sulfated simultaneously at 900°C with a simulated combustion gas (0.25% SO_2, 17% CO_2, 5% O_2, 5% H_2O and balance N_2) flowing over the sample surface at a velocity of about 10cm/sec. This velocity was predetermined to be high enough to minimize gas film diffusion rate. The steam in the reactant gas was generated by bubbling the inert carrier gas (N_2) through a water bath before entering the preheater. The bubbler was jacketed and water was circulated in the jacket from a constant temperature water bath.

A quartz fluidized-bed sulfator was used for studies under more realistic conditions. The fluidized-bed was 40-mm Id, 11-cm long with a 56-mm ID, 12-cm long free board and a quartz fitted plate as the gas distributor. Solid samples were loaded into the bed and were fluidized with a simulated combustion gas. The gas was first preheated to 800°C by passing through a quartz tube packed with alumina chips and housed in a tubular furnace. The steam was carried by nitrogen gas prior to entering the preheater. The preheated gas was heated to the operating temperatue (900°C) in the fluidized bed by the sulfator

furnace. The pretreated samples were dropped into the preheated reactor with preheated sulfating gas mixture flowing through it. After each run, the $CaSO_4$ contents in the solid samples were determined by the thermal decomposition of about 100 mg sulfated stone (16/20 mesh) in N_2 flow at 1300°C.

(b) Regeneration System

Materials

The sulfated Greer limestone was from our fluidized-bed sulfator and the size used in the regeneration was 16/20 Tyler mesh. The fly ash from Sewickley coal was kindly supplied by Argonne National Laboratory from the secondary cyclone of their 6-in. combustor. The fly ash contained 8.55% carbon, 8.91% Ca^{++}, 2.89% S, 8.49% $SO_4^{=}$, 3.76% Mg^{++} and 1.09% $CO_3^{=}$.

Apparatus and Procedure

In TGA studies, the Mettler TA-1 was used for the regeneration rate measurements at 1000°C. A shallow quartz sample holder with an area of about 1.5 cm^2 was used in the experiments. The materials were regenerated in a flow of dry and purified N_2 at a velocity of about 8 cm/sec; a velocity high enough to ensure that the partial pressure of SO_2 was zero and there were no mass transfer effects on the rate. Nitrogen gas was passed through a tube packed with copper turnings held at 600°C for residual oxygen removal before flowing over the sample.

The apparatus and experimental procedures of the rotary kiln were described in our quarterly progress report No. 6.

Results and Discussion

The sulfation rates of the Greer limestone were compared with those coated or impregnated with ferric sulfate in TGA. Each experiment lasted for five hours. Blank test was run under calcination condition (17% CO_2, 5% O_2, 5% H_2O and balance N_2 at 900°C) without SO_2 to provide the baseline for sulfation in this simultaneous calcination and sulfation experiment. Iron sulfate was also decomposed to iron oxide at the initial stage of the experiment. As shown in Figure 8, the sulfation rate of the Greer limestone impregnated with ferric sulfate is higher than that of the uncoated Greer limestone.

With the fluidized-bed sulfator, lime utilization was measured by the uptake of SO_3 after five hours of simultaneous calcination and sulfation. Twenty grams of the pretreated Greer limestone (16/20 mesh) were sulfated at 900°C with 0.25% SO_2, 5% O_2, 5% steam and balance N_2 at 3 ft/sec superficial velocity. The SO_3 contents in the reacted samples determined by thermal decomposition are as follows:

Untreated Greer limestone: 14.9%

Greer limestone with 0.5% $Fe_2(SO_4)_3$ impregnated: 18.7%

Greer limestone with 1.0% $Fe_2(SO_4)_3$ impregnated: 20.7%

The results show that lime utilization is enhanced by about 20% with 0.5% $Fe_2(SO_4)_3$ impregnated Greer limestone and about 30% with 1.0% $Fe_2(SO_4)_3$ impregnated.

Other iron salts which can be readily dissolved in water and decomposed to iron oxide below combustion temperature are sulfite,

oxalate, acetate, formate, and nitrate. Nitrates are in theory useful but in practice provide noxious nitrous gases upon decomposition, and, therefore, its use is questionable. Work is in progress on the effects of using different kinds of salts.

Iron is employed in view of its relatively low cost and its existence in significant amounts in coal ash. Salts of other transition metals, preferrably Co and Ni, have also been examined. Six samples of Greer limestone to which salts were added were heat treated in N_2 at 900°C for two hours. The treated samples were tested for their sulfation capabilities in TGA (duPont 951) under identical conditions. The results are as follows:

Sample No.	Coating Additions	Percent Sulfation
1	Uncoated	24.1%
2	2% $Fe_2(SO_4)_3$	28.8%
3	2% $FeSO_4 \cdot 7H_2O$	26.3%
4	2% $CoSO_4 \cdot 7H_2O$	25.6%
5	2% $NiSO_4 \cdot 7H_2O$	25.6%
6	1% $Fe_2(SO_4)_3$ + 1% $CoSO_4 \cdot 7H_2O$	27.0%
7	1% $FeSO_4 \cdot 7H_2O$ + 1% $CoSO_4 \cdot 7H_2O$	26.1%

The sulfates/sulfites were pre-decomposed before TGA experiments. The results of SO_2 absorption indicate that sample No. 2 showed a higher level of absorption compared to sample No. 1, while sample Nos. 3, 4, and 5 showed measurable improvement over the uncoated sample No. 1.

Iron oxide also catalyzes regeneration. Figure 9 shows that in TGA, with 2% Fe_2O_3 physically added, the rate of reaction

$$3CaSO_4 + CaS \rightarrow 4SO_2 + 4CaO$$

(the controlling step of regeneration of CaO) is increased greatly in the first five minutes.

The regeneration rates for the sulfated Greer limestones and the sulfated Greer limestone impregnated with iron oxide are compared in Figure 10. All the regeneration experiments were done with high flow nitrogen. The samples from our fluidized-bed sulfator are regenerated with fly ash containing unburnt carbon. The rate of regeneration for the sulfated Greer limestone with 1.1% Fe_2O_3 coated was higher.

Work on kiln regeneration of the sulfated Greer limestone impregnated with iron oxide is in progress. Figure 11 shows particle size distributions of the sulfated Greer limestones with and without iron oxide coated after five hours of sulfation in the fluidized-bed sulfator. It appears that iron oxide impregnation did not weaken the sulfated particle.

In order to relate the porosity measurements to sulfation reactivity, samples of the Greer limestone with and without iron oxide coating were calcined under identical conditions (1 hour at 900°C in N_2). The porosity curves of accumulated pore volume versus pore diameter for the two samples are presented in Figure 12. Unlike the addition of NaCl to limestone in which the average pore diameter shifts to a large size upon calcination[2], impregnating the limestone with iron oxide did not change the size of the average pore diameter, but caused a decrease in total porosity. It is believed that most sulfation takes place in larger pores ($\geq$ 0.3 μm) and that pores smaller than 0.3 μm are relatively easy to be closed upon sulfation.[3] The enhancement of sulfation by impregnating with iron oxide may be due to a chemical

effect rather than a pore-enlargement effect. The other evidence is that the sulfation rates at a higher pressure (10 atm) for Greer lime were not increased significantly by impregnating it with iron oxide. Results and discussion of the high pressure measurements were given in the previous quarterly report (No. 7).

D. Reactivity of the Reconstructed $CaSO_4$ (M-S. Shen, R. T. Yang)

It has been suggested by Dr. W. E. Winsche of this Laboratory that the morphological and structural changes undergone in the following scheme may effect a higher or different reactivity of the sulfate for regeneration:

$$CaSO_4 + 2C \rightarrow CaS + 2CO_2$$
$$\downarrow + 2O_2$$
$$CaSO_4$$

Experiments are being conducted to examine this possibility and the information may be useful for advanced applications. $CaSO_4$ was first converted to CaS by carbon at 900°C in nitrogen flow and subsequently the CaS was reacted with oxygen (20% O_2, 80% N_2) to form $CaSO_4$. The sample material studied here was Baker AR grade, 270/400 mesh size. The reactivity of the original $CaSO_4$ and the reconstructed $CaSO_4$ were compared via the following reaction:

$$CaSO_4 + CO \rightarrow CaO + CO_2 + SO_2$$

The result shows that the starting temperature of the above reaction for the reconstructed $CaSO_4$ is about 50°C lower than that of the original $CaSO_4$. This indicates that the reactivity of the

reconstructed $CaSO_4$ is indeed higher.

E. High Temperature Regeneration Chemistry (J. M. Chen, F. B. Kainz, G. Farber, and R. T. Yang)

(1) Introduction

The reaction schemes currently being considered for regeneration of the sulfated lime from fluidized bed combustor can be written in the general form:

$$4CaSO_4 + 2R \rightarrow 4CaO + 4SO_2 + 2RO_2 \quad (22)$$

Where R is the reductant. The reductants being considered are CO, C, H_2, and CH_4. The success of using the above process for lime regeneration on a laboratory scale has been reported in a number of references.[2,5,6,7] In all these processes, the reaction temperatures were in the range of 950°C to 1200°C.

The main objectives of a regeneration process are as follows: (1) to obtain high regenerability with a short solid residence time, (2) to obtain a high SO_2 particle pressure (high concentration) for purposes of conversion to H_2SO_4 or elemental sulfur, (3) to retain lime reactivity for sulfation. Rates of regeneration and SO_2 concentrations increase with increasing temperature, but the reactivity of the regenerated lime decreases with increasing temperature. The latter effect becomes more pronounced with temperatures higher than 1000°C due to sintering. Because of this effect selection of the optimal regeneration temperature is an important task.

Using reductants to regenerate the sulfated lime, reaction (22) has been found to proceed in two consecutive steps[11]

$$CaSO_4 + 2R \rightarrow CaS + 2RO_2 \quad (23)$$

$$CaS + 3CaSO_4 \rightarrow 4CaO + 4SO_2 \quad (24)$$

In this two-step reaction mechanism, the second common step, reaction (24) is the rate controlling step, especially at low temperatures. That is, three moles of $CaSO_4$ react with one mole of CaS, formed from the reduction reaction (23), to produce CaO and SO_2. Thus, thermodynamics of reaction (24) dictates maximum attainable SO_2 concentration in the gas phase; its value increases from 0.05 atm at 950°C to 0.1 atm at 1000°C and to 0.5 atm at 1100°C. Our experimental results[11] showed that more than 7% SO_2 composition at 1 atm (0.07 atm) could be obtained at 1000°C regeneration temperature (22) which is only 30% below equilibrium.

In the SO_2-rich reacting systems, reaction (24) may not be the sole reaction occurring. Both CaS and CaO may also interact with SO_2 gas. Thermodynamics indicate that the following reactions are feasible at high temperatures:

$$1/4\ CaS + 3/4\ CaSO_4 \rightleftarrows CaO + SO_2 \quad (25)$$

$$2/3\ CaO + SO_2 \rightleftarrows 2/3\ CaSO_4 + 1/6\ S_2 \quad (26)$$

$$CaS + 2SO_2 \rightleftarrows CaSO_4 + S_2 \quad (27)$$

$$2CaS + SO_2 \rightleftarrows 2CaO + 3/2\ S_2 \quad (28)$$

$$3/2\ CaS + 1/2\ CaSO_4 \rightleftarrows 2CaO + S_2 \quad (29)$$

$$CaSO_4 \rightleftarrows CaO + SO_3 \quad (30)$$

The equilibrium constants, K's for the above reactions are plotted against 1/T in Figure 13. Because of the possible occurrence

of the above reactions, it is important to understand the chemistry of high temperature lime regeneration process.

It is worth mentioning here that the calcium sulfide and sulfate reaction has been used earlier for sulfuric acid manufacturing[8,9] in which producing an SO_2-rich off gas was the main objective, and the temperature effect on lime reactivity was not of importance. However, to employ the same reaction for the purpose of recycling lime sorbents, lowering regeneration temperature is most desirable. Since the available information about the chemistry and rates up to now are very scarce, it is the objective of this work to investigate this high temperature chemistry. The reactions considered are CaS with $CaSO_4$, CaO with SO_2, and CaS with SO_2.

(2) Results

(a) CaS With $CaSO_4$

Previous experiments done by Shen, presented in BNL quarterly report No. 7, in which a CaS pellet and a $CaSO_4$ pellet, separated by a quartz ring, were heated to 900°C and 1100°C for two hours. The product samples were found to remain in their original shapes but both CaS and $CaSO_4$ had been converted to CaO. This result indicated the existence of gas intermediates to carry out the apparent solid-solid CaS and $CaSO_4$ reaction.

Based on the above finding, the reaction mechanism for the reaction is postulated as:

$$3CaSO_4 \rightarrow 3CaO + 3SO_x + 3\left(\frac{3-x}{2}\right) O_2 \quad (0 \leq x \leq 3) \tag{31}$$

$$CaS + 3SO_x + 3\left(\frac{3-x}{2}\right) O_2 \rightarrow CaO + 4SO_2 \quad (32)$$

That is, the gas intermediate is produced from $CaSO_4$ decomposition and then the gas cracks CaS to form CaO and SO_2. The possible chemical compounds considered as gas intermediates are O_2, SO_2, and SO_3. To determine which gas is the controlling intermediate, the reaction product of CaS with each of the gases was measured. The results are listed in the following:

2.a.1. CaS with SO_2

A Cahn thermobalance was used for measurements. Results of the weight changes of CaS with 8% SO_2 in N_2 at 1000°C are given in Figure 14. The samples gained weight rather than lost weight. This weight apparently indicated that SO_2 was not the gas intermediate. X-ray diffraction analysis showed formation of $CaSO_4$.

2.a.2. CaS with

The reaction products between calcium sulfide and oxygen have been known to be calcium sulfate at low temperatures; but to be calcium oxide and sulfur dioxide at high temperatures. Since CaS with $CaSO_4$ reaction starts from 900°C, if oxygen is the intermediate, the reaction between CaS and O_2 should form CaO and SO_2 at these temperatures. Experimental results of CaS with O_2 (20% in N_2) at 1000°C are shown in Figure 14. Again, the CaS sample gained weight from oxygen gas. X-ray diffraction also indicated the formation of $CaSO_4$.

2.a.3. CaS with SO_3

Before experimenting SO_3 with CaS reaction, the thermodynamics of the following reaction was examined:

$$CaS + 3SO_3 \rightarrow CaO + 4SO_2 \qquad (33)$$

Plots of equilibrium constant versus reciprocal temperature are given in Figure 15; the high equilibrium constant values strongly suggest the feasibility of this reaction. For instance, at 1000°C, the equilibrium SO_3 partial pressure for $CaSO_4$ decomposition is 0.8×10^{-7} atm. With this value, the equilibrium partial pressure of SO_2 is 0.093 atm.

The reaction of CaS with SO_3 was measured in a tubular reactor. Argon was used as the carrier gas which bubbled through an SO_3 liquid container (see Figure 25) to the CaS sample (pelletized) containing reactor. To study this reaction, care was taken to avoid the possible reaction between CaS and $CaSO_4$ to produce CaO (if $CaSO_4$ could be formed from CaS + SO_2), which may create misleading information. Since practically no reaction between CaS and $CaSO_4$ could occur at temperatures below 900°C, the reaction temperature for CaS + SO_3 was controlled at 800°C. Also because SO_3 can react rapidly with CaO to form $CaSO_4$ (unless the SO_3 partial pressure is less than equilibrium decomposition value, $P_{SO_3} < 10^{-8}$ atm at 800°C), to prevent CaO formed through reaction (33) from being converted to $CaSO_4$, SO_3 was pulsed into the reactor.

Two experiments were made with pulsing time intervals of 1 sec and 15 sec and with about 0.5% SO_3 in the gas stream (determined from

the partial pressure of SO_3). The product pellets were then analyzed by thymolphthalein indicator solution (pH 9.3-10.5). When a few drops of thymolphthalein solution were applied to the surface of these pellets, the color of product pellets immediately turned blue. However, the samples of pure CaS and pure $CaSO_4$ remained their own colors. This indicated that CaO was contained in the solid sample. X-ray diffraction also showed that both CaS and $CaSO_4$ also existed in the sample. The $CaSO_4$ content is believed to be due to the CaO and SO_3 reaction.

From the above investigation, it is clear that SO_3 can react with CaS to form CaO. In the sulfide-sulfate reaction, SO_3 is produced through the sulfate decomposition, its partial pressure is less than the equilibrium value at any given temperature. Because of this, the product CaO formed from the CaS SO_3 reaction will not be converted back to $CaSO_4$. Hence, it can be concluded that SO_3 is the gas intermediate for calcium sulfate-sulfide reaction. Thus, the rate mechanism is:

$$3CaSO_4 \rightarrow 3CaO + 3SO_3$$

$$CaS + 3SO_3 \rightarrow CaO + 4SO_2$$

2.a.4. Reaction Kinetics

After establishing the reaction mechanism, work was conducted to determine the rate controlling step for the sulfide-sulfate reaction. To do this, one can see that if the sulfate decomposition, reaction (30), is rate controlling, by keeping a constant amount of $CaSO_4$, the weight change with respect to time will not be effected by the CaS amount,

provided enough CaS is present in the mixture for total conversion. However, if the CaS reaction with the gas intermediate is rate controlling, this rate will be affected by the CaS content. With the above thinking in mind, experiments were conducted in a Cahn TGA apparatus. Samples of CaS and $CaSO_4$ were mixed in a sample pan, and the weight changes of the sample were followed. The experimental conditions were as follows:

Temperature: $1000^{o}C$

Sample:

reagent $CaSO_4 \cdot 2H_2O$ ($\frac{270}{400}$ mesh)

reagent CaS ($\frac{270}{400}$ mesh)

Gas composition: pure N_2

Gas flow rates: 1000 sccm

Figure 16 gives the experimental results. With a fixed amount of $CaSO_4$ (27 mg), the weight loss rates for the samples with 4.8 mg CaS, and 9.6 mg CaS are essentially the same (4.8 mg CaS is the stoichiometric amount for 27 mg $CaSO_4$). Reducing the $CaSO_4$ content with the same amount of CaS gives slower rates. From these data, it is clear that calcium sulfate decomposition is the rate controlling step.

One comment must be mentioned here about the thermal decomposition of $CaSO_4$. Numerous investigations of this reaction have been made and have recently been reviewed by Colussi and Longo.[10] The reaction rates of $CaSO_4$ without CaS presence were found to be much lower than with CaS present under the same reaction conditions. The reason for this is that the equilibrium decomposition partial pressure of SO_3 is

very low, e.g. 0.8×10^{-7} atm at 1000°C. The gases evolved from the $CaSO_4$ decomposition tend to hinder the process, in accordance with the laws of chemical equilibrium. With the presence of CaS, the evolved gases are continuously removed, the equilibria of reaction (30) are quickly displaced to the right. This causes a change in the temperature at which the beginning of decomposition can be experimentally determined. Therefore, the measureable reaction temperature for CaS and $CaSO_4$ is about 900°C, while that for $CaSO_4$ decomposition is above 1100°C. This may also be the reason why the decomposition rates of $CaSO_4$ were enhanced under vacuum or with steam.

E. Reaction Kinetics

Figure 17 depicts the results of conversion, X, versus time for sulfide-sulfate (sizes: $\frac{270}{400}$ mesh) reactions at temperatures of 900°C, 950°C and 1000°C. The flow rates for these results were controlled at 1000 sccm. Plots of log (1-x) versus time is shown in Figure 18, are substantially linear (because this apparent solid-solid reaction begins to lose weight before reaching isothermal measured temperatures, these straight lines would not necessarily cross the vertical axis at value 1 at time zero). These linear results indicate that the reaction order with respect to solid concentration is first order.

By expressing the reaction rates as

$$\frac{dS}{dt} = -\bar{k}S$$

where S is the solid concentration and $\bar{k}$ is the rate constant, including effects of gas concentration on rates. The values of $\bar{k}$ can be obtained from the slopes of log (1-x) versus time chart (Figure 18). Using an

Arrhenius expression, the temperature dependence of $\bar{k}$ was determined from the slope of log $\bar{k}$ versus reciprocal temperature plot, shown in Figure 19. The value was 82 kcal/mole.

In most of decomposition reactions in which gas products are formed, reaction rates have been found to be proportional to the difference between the equilibrium partial pressure, P_e, and the bulk gas partial pressure, P, i.e.,

$$\bar{k} \alpha k(P_e - P)$$

In these experiments pure N_2 gas was flowing through the reactor. Thus, P is zero. Since P_e is dependent upon temperature, the measured temperature dependent value for $\bar{k}$ is the summation of those for both $\bar{k}$ and P_e. The temperature dependence of P_e for the sulfate-sulfide reaction is 58 kcal/mole (determined from thermodynamics). Therefore, the activation energy for k is 24 kcal/mole. This magnitude of activation energy assures that the measured rates were free from mass transfer effects.

Although the sulfide-sulfate reaction is a two-step process, since the reaction between sulfide with gas intermediate is very much faster than the sulfate decomposition it is very likely that the gas intermediate formed through decomposition reaction can totally react with sulfide to produce SO_2 (which was found true as the maximum measured weight loss corresponded to the theoretical value for 100% sulfate-sulfide reaction). Under this case, the difference between SO_2 equilibrium partial pressure for sulfate-sulfide reaction and SO_2 gas partial pressure can

be used as the driving force for the reaction. Therefore, the kinetics can be written in the following form:

$$\frac{ds}{dt} = -k(Pe_{SO_2} - Pg_{SO_2}) \; S$$

k was calculated to be

$$k = 3.3 \times 10^2 \exp\left(\frac{-12,078}{T(K)}\right) , \frac{1}{atm\text{-}sec}$$

It should be mentioned here that attempts were also made to determine the relationship between reaction rates and SO_2 concentration. To do this, SO_2 gas was mixed with N_2 before flowing into reactor. Results are shown in Figure 20; initially the sample lost weight, followed by gaining weight as time progressed. This indicates that not only sulfide-sulfate reaction occurred, but also other reactions, such as CaS + SO_2 and CaO + SO_2, were competing. Therefore, the rate dependence on SO_2 concentration could not be extracted from the above experimental results.

(b) CaO With SO_2

Reaction between CaO and SO_2 was measured in the Cahn TGA apparatus, in which about 20 mg of CaO powder samples were exposed to constant gas composition (SO_2 in N_2) with a fixed total flow rate of 1000 sccm. In all these measurements, SO_2 partial pressures were kept below the equilibrium values of sulfide-sulfate reaction (reaction 25) to prevent formation of CaS whose reaction with SO_2 might compete with the CaO reaction. The product samples were analyzed by x-ray diffraction, indicating the formation of $CaSO_4$. These results confirmed the occurrence of reaction (26). That is, calcium oxide

reacts with SO_2 to form $CaSO_4$ and elemental sulfur. After determining the reaction product, the measured weight gain with respect to time could then be used to determine the extent of conversion versus time and then plot in Figure 21.

Figure 21 shows that at constant SO_2 concentration the measured reaction rates decrease with increasing temperature. To explain this, one should examine the thermodynamics of this reaction. Reaction (26) is an endothermic reaction. Increasing temperatures reduces the equilibrium constants. With 0.04 atm SO_2 partial pressure, the equilibrium partial pressures for elemental sulfur (S_2 varies from 0.6×10^{-4} atm at 950°C, to 0.3×10^{-5} atm at 1000°C and to 0.1×10^{-8} atm at 1100°C. It is apparent that under the operating conditions the evolved gas (S_2) from the reaction hindered the progress of the reaction resulting in slower rates at higher temperatures. Therefore, the measured data were not in the chemical reaction control region.

(c) CaS with SO_2

Reaction between CaS and SO_2 was measured under the same operating conditions as for CaO with SO_2 measurements. However, in most of these measurements, the SO_2 partial pressures were kept above the equilibrium SO_2 partial pressure for sulfate-sulfide reaction. The reason for this was to prevent the interference of the reaction between CaS and $CaSO_4$, formed through CaS and SO_2 reaction. The product samples were analyzed by x-ray diffraction, indicating that the samples contained CaS and $CaSO_4$ but no CaO. Hence, it can be concluded that reaction (27) rather than (28) occurring. That is, CaS reacts with SO_2 to form $CaSO_4$ instead of

CaO. Results of the measured weight changes with respect to time were then converted to degree of conversion versus time. Figures 22 and 23 show the effects of temperature and SO_2 concentrations on reaction rates respectively. By plotting initial rates versus SO_2 concentration on a log-log scale in Figure 24 the reaction was found to be 1.5 order with respect to SO_2 concentration.

The effects of temperature and pressure on the amount of sulfur vapor in the gaseous atmosphere in equilibrium with a system of solid phases, $CaSO_4$-CaS-CaS and coexisting with SO_2 and S_2 were given by Fleck.[9] Because both CaS and SO_2, and CaO and SO_2 are exothermic reactions, for a given SO_2 partial pressure, the proportion of sulfur vapor decreases with increasing temperatures. Both CaO with SO_2 and CaS with SO_2 reactions are undesirable in the regeneration process due to $CaSO_4$ formation through these reactions. However, because of the low values of thermodynamic limits that CaS + SO_2 and CaO + SO_2 reactions can proceed, these reactions do not alter the feasibility of the above regeneration processes. Nevertheless, consideration of the above reactions may become important in design or optimization of regeneration reactors.

F. Kinetics of the CaO-SO_3 Reaction (J. Chen, G. Farber, F. Kainz, and R. T. Yang)

Work is being conducted to measure the reaction kinetics of CaO with SO_3 in comparison with CaO with SO_2 and O_2. The objective of this study is to eludcidate the reaction mechanism of CaO sulfation. Understanding the mechanism will be useful in developing new processes for improving the reactivity and utilization of lime for

sulfation in fluidized bed combustion technology.

During this quarter the apparatus for the reaction rate measurements has been set up and some preliminary experiments have been made. The apparatus is shown in Figure 25.

Liquid SO_3 (mixture of β and r form) was contained in a bubbler. The bubbler was submerged in a water bath whose temperature was controlled to be within 0.05°C by a temperature controller (Lauda k-2/R). The SO_3 partial pressure with respect to temperature[12] is given in Figure 26. By controlling SO_3 liquid temperature, the SO_3 concentration in the inlet gas stream could be regulated. An infrared lamp was used to heat the tubing connected to the bubbler to prevent SO_3 vapor solidification and flow pluggage. The SO_3 vapor was carried by an inert gas stream (Argon) which was merged with a pure inert gas stream to dilute SO_3 concentration before entering a tubular quarts reactor. Flow rates of the gas streams were regulated by rotameters. The reactor consisted of a gas preheating zone, which contained packed alumina beads, and a reaction zone in which solid reactant samples were placed. The heat for the reactor was supplied by a furnace. The temperature was controlled within $\pm$ 5°C by a transformer.

The outlet gas stream flows through a gas sampling bulb and to water containing bubblers for SO_3 scrubbing. The composition of the gas sample was then analyzed by mass spectrometry.

The flow connections for this system were made of stainless steel tubing (type 316), and Pyrex glass. Teflon tubing was used only for the connection to the reactor. However, the connections to

the SO_3 container were all stainless steel tubing. For the glass joints KEL-F grease was used. No attack of SO_3 on the connections in the system was observed.

The sulfate content in the product samples were analyzed by a Barium sulfate precipitation method.

(a) Preliminary Results

To test the performance of the apparatus, four runs of SO_3 with CaO reaction for different reaction periods were made. The operating conditions were as follows:

Temperatures

reactor: $850 \pm 5^{o}C$

SO_3 bubbler: $28 \pm 0.05^{o}C$

Flows

F1 (through bubbler): 100 cc

F2 (dilute stream): 1000 cc

Solid Samples

Calcined Greer lime (16/20 mesh): 100 mg

Results of sulfate content in the solid samples were

Time (min):	2	5	10	20
$SO_4^{=}$ wt%:	23%	26%	33%	33%
CaO utilization:	23%	27%	36%	36%

The SO_3 concentration, however, could not be detected by mass spectrometric analysis. This was because SO_3 could react with trace H_2O and stayed on the walls of the sampling bulb. Consequently, it was decided that converting SO_3 to H_2SO_4 and using titration method for SO_3 analysis was necessary. The absorption device for titation measurements, however, must be capable of separable absorption of SO_3 and SO_2, from SO_3 decomposition, in order to obtain accurate analysis. To do this, two absorbers containing about 80% isopropanol in distilled water will be connected in series to absorb SO_3. Between these two absorbers a glass impinger is fused to stop H_2SO_4 aerosols. The isopropanol solution is used to retard SO_2 absorption in water. Following these two SO_3 absorbers, two additional absorbers containing hydrogen peroxide in water solution will be used to absorb SO_2.[13] This absorption set-up is currently under construction and will be tested in the next quarter and the reaction rates between CaO with SO_2 and O_2 will then be measured for comparison.

(b) Acknowledgements

Supply of SO_3 obtained from Dr. R. Dietz and Ms. M. Greene was deeply appreciated. The advice from them in handling this nasty material is most helpful.

G. Cyclic Use of Zinc Oxide as a Sorbent for Hot Fuel Gas Desulfurization (C. L. Steen and R. T. Yang)

(1) Introduction

The cyclic use of solid sorbents such as limestone, dolomite, and metal oxides for the control of sulfur emissions has become an area of intensive research. The primary problem associated with the

use of such compounds is an incomplete or energy intensive regeneration reaction.

Thermodynamic studies indicate that zinc oxide is an especially effective sorbent for H_2S.[14] Studies also indicate that the regeneration of zinc oxide from zinc sulfide is feasible at the temperatures of interest in coal gasification processes.[15]

The objective of this study is to determine the feasibility of the use of zinc oxide as a regenerable sorbent for H_2S and COS under conditions of interest in coal gasification processes.

(2) Thermodynamic Considerations

Thermodynamics of the following reactions were considered:

$$ZnO + H_2S \rightarrow ZnS + H_2O \quad (34)$$

$$ZnO + COS \rightarrow ZnS + CO_2 \quad (35)$$

$$ZnS + \frac{3}{2} O_2 \rightarrow ZnO + SO_2 \quad (36)$$

Data are given in Table 1, and a plot of ln Kp versus $\frac{1}{T}$ is shown in Figure 27. All reactions are exothermic, and have high equilibrium constants.

The regeneration reaction (36) was compared with the reaction:

$$FeS + \frac{3}{2} O_2 \rightarrow FeO + SO_2 \quad (37)$$

which is part of a cyclic process used by Battelle.[11] The ΔH_{rxn} values shown in Figure 28 do not show any clear advantage of the ZnO system over the FeO system. However, the FeO regeneration reaction (37) has a high activation energy, and must be careied out at high temperatures. If the ZnO regeneration reaction (36) has a lower activation

energy, this system would be favored.

A review of the literature indicated several potential problems in the use of zinc oxide. These are outlined below.

(1) The presence of water vapor in the gas may affect the rate sulfation.[17]

(2) A small amount of $ZnSO_4$ may be formed in the regeneration process as a result of reaction with SO_2.[18,19]

(3) Zinc vapor may be formed in a reducing atmosphere.[20]

As the formation of zinc vapor would make a hot gas scrubbing process using zinc oxide unworkable, the thermodynamics of the following reactions were considered:

$$ZnO + H_2 \rightarrow Zn + H_2O \quad (38)$$

$$ZnO + CO \rightarrow Zn + CO_2 \quad (39)$$

The results, given in Table 2, indicate that zinc vapor may form in significant quantities.

(3) Results and Discussion

All experiments were performed on a modified Sartorius TGA apparatus under conditions of interest in coal gasification processes. Experimental conditions are listed in Table 3.

Results shown in Figures 29 and 30, indicate that both the reaction with H_2S (34) and the regeneration reaction (36) are quite rapid at atmospheric pressure and temperatures greater than 800°C. X-ray examination of the regenerated zinc oxide showed no lattice distortions indicating that the product is 100% ZnO.

Unfortunately, the formation of zinc vapor in a hydrogen atmosphere is an extremely rapid process at high temperatures as shown in Figure 31. Since the concentrations of H_2 and CO overwhelm the concentrations of H_2S and COS in a gasifier exit stream, the use of zinc oxide as a sorbent is unworkable.

(4) Conclusions

On the basis of rates of sulfidation and regeneration, zinc oxide is a good candidate for use in fuel gas scrubbing process at moderate temperature. The rate of formation of zinc vapor in a reducing atmosphere temperatures higher than c.a. 700°C, such as exits in a gasifier exit stream, is sufficiently rapid to make this process unworkable.

We thank Dr. W. E. Winsche for bringing the subject matter to out attention.

H. Process Design and Evaluation (A. S. Albanese and M. Steinberg)

An economic comparison between an AFBC once through limestone sorbent system and BNL's regenerative sorbent system (kiln) with production of 1) sulfuric acid, and 2) sulfur from the SO_2 rich regenerator off-gas has been initiated. The comparisons will be made for a 600 MWe plant assuming a limestone cost of $10 per ton and a solids disposal cost of $3 per ton. Parametric studies will be developed to indicate the sensitivity of the comparisons to limestone, disposal and capital costs, and to byproduct value.

References

1. R. T. Yang, M-S. Shen, and M. Steinberg, Catalytic sulfation of lime with iron compounds and coal ash, Env. Sci. Tech., in press.

2. A. Jonke et al., Supportive studies in fluidized-bed combustion, Annual Report, Argonne National Laboratory, Argonne, Ill., EPA-600/7-77-138 (1977).

3. M. Hartman and R. W. Coughlin, Reactions of sulfur dioxide with limestone and the influence of pore structure, Ind. Eng. Chem. 13 (3), 248 (1974).

4. R. T. Yang, et al., Regenerative process for desulfurization of hot combustion gases, Quarterly Report No. 6, Brookhaven National Laboratory, July 1-September 30, 1977.

5. R. T. Yang, J. M. Chen, G. Farber, M. Shen and M. Steinberg, Regeneration of lime-based sorbents in a kiln with solid reductants, Proceeding of the 5th Inter. Conf. on FBC, Washington, D. C. December 12, 1977, in press.

6. E. T. Turkdogen, J. V. Vinters, Trans. Inst. Mining and Metallurgy, in press (1977).

7. T. D. Wheelock and D. R. Boylan, Ind. Eng. Chem. 52, 215 (1960).

8. W. Q. Hull et al., Ind. Eng. Chem. 49, 1204 (1957).

9. A. Fleck, Chem. Ind. (London) 1184 (1952).

10. I. Colussi and V. Longo, Cements 71, 75 (1974).

11. R. T. Yang et al., Regenerative process for desulfurization of hot combustion and fuel gases, Quarterly Report No. 7, Brookhaven National Laboratory, October 1-December 31, 1977.

12. T. Moeller, Inorganic Chemistry, Chapt. 14, John Wiley and Sons (1952).

13. R. Dietz, Private communication, Brookhaven National Laboratory (1978).

14. P. R. Westmoreland, J. B. Gibson, and D. P. Harrison, Environ. Sci. and Tech., Vol. 1 11, No. 5 (1977), pp. 488-491.

15. K. Natesan and W. O. Philbrook, Metall. Trans. 1, 1353 (1970).

16. K. S. Murthy, ACS Division of Fuel Chemistry (preprints) Vol. 20, No. 4 (August 24-29, 1975) p 238.

17. W. R. Gutmann and J. H. Wright, U. S. Patent No. 3,441,370.

18. R. Dimitrov and A. V. Vanyukov, Chem. Abstracts, No. 73:29415g.

19. A. V. Spasov and A. Lenchev, Chem. Abstracts, No. 72:83382 m.

20. W. W. Bodle and K. C. Vyas, Oil and Gas Journal, p. 73, August 26, 1974.

Table 1

THERMODYNAMIC DATA

$$ZnO + H_2S \rightarrow ZnS + H_2O \quad (1)$$

$$ZnO + COS \rightarrow ZnS \pm CO_2 \quad (2)$$

$$ZnS + 3/2O_2 \rightarrow ZnO + SO_2 \quad (3)$$

Reaction Number	Temperature (°K)	ΔG_{rxn} (kcal/mole)	ln Kp
(1)	1255	-18.526	7.429
	1311	-18.599	7.140
	1422	-18.719	6.625
(2)	1255	-25.889	10.398
	1311	-25.930	9.954
	1422	-26.002	9.203
(3)	1255	-81.942	32.860
	1311	-80.809	31.021
	1422	-78.558	27.803

Table 2

THERMODYNAMIC DATA

$$ZnO + H_2 \rightarrow Zn + H_2O \quad (5)$$

$$ZnO + CO \rightarrow Zn + CO_2 \quad (6)$$

Reaction Number	Temperature (°K)	ΔG_{rxn} (kcal/mole)	ln Kp
(5)	298	19.399	-32.746
	1255	8.084	- 3.240
	1478	0.406	- 0.685
(6)	1255	9.215	- 3.694
	1311	7.664	- 2.942
	1478	3.065	- 1.044

Table 3

EXPERIMENTAL CONDITIONS

Type of Reaction	Temperature Range	Gas/Mole % (in N_2)
Sulfidation	650-810°C	H_2S/0.4%
Regeneration	800-900°C	O_2/8.3%
Reducing Atmosphere	800°C	H_2/45%

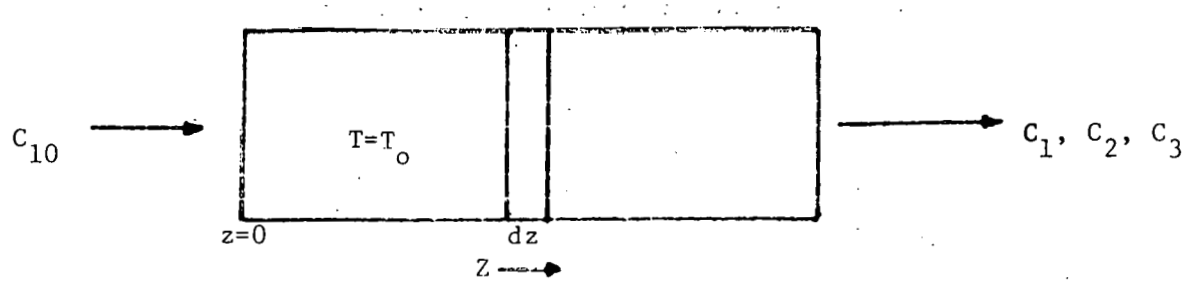

Figure 1. Schematic of rotary kiln regenerator.

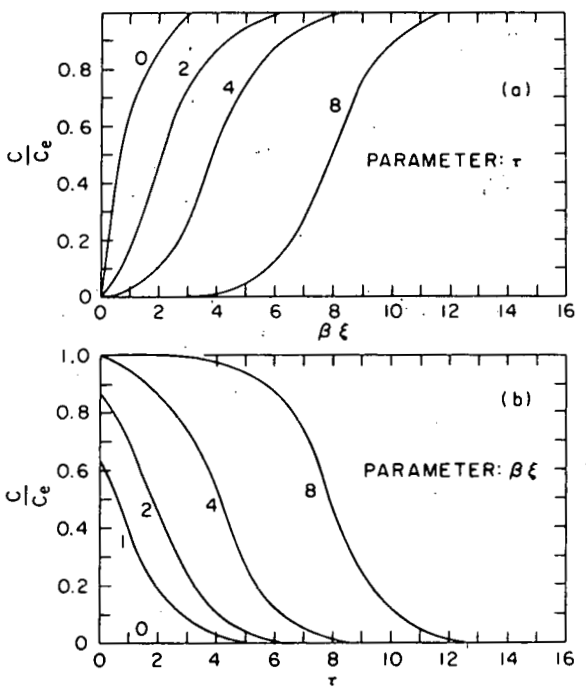

Figure 2. Variations in sulfur dioxide concentration with respect to bed length (2a), and reaction time (2b), respectively (Equation (12)).

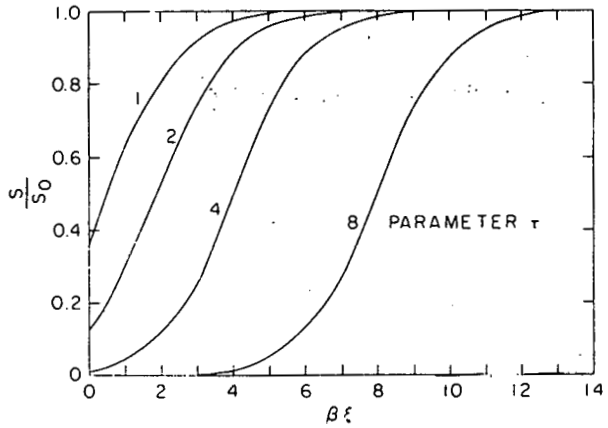

Figure 3. Variation in solid concentration down the bed (Equation (13)).

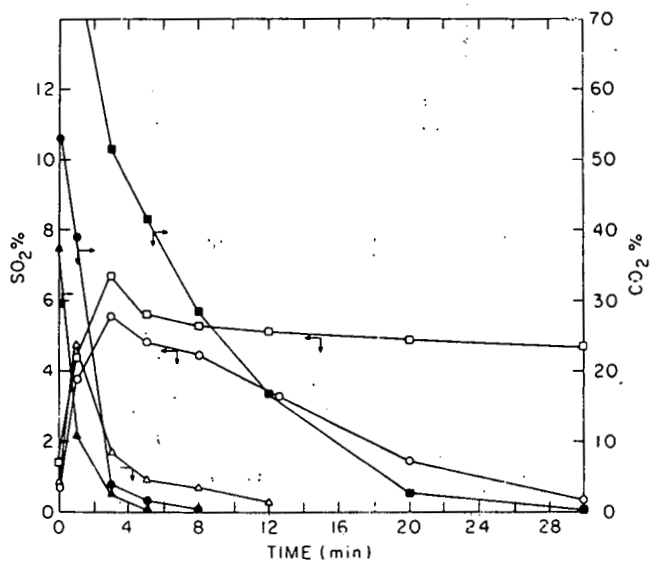

Figure 4. Exit SO_2 and CO_2 compositions versus time at 1000°C; flow rates, 10 sccm (,), 50 sccm (0,0), 150 sccm (Δ, Δ).

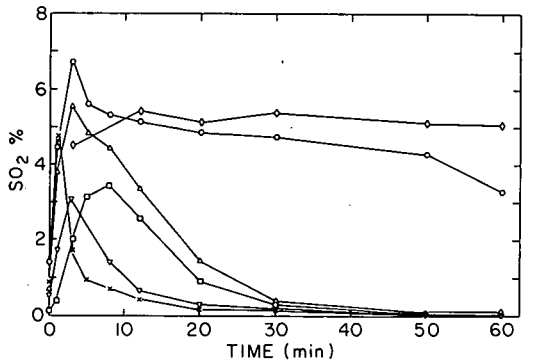

Figure 5. Exit SO_2 composition versus time for various flow rates at 1000°C; 5 sccm (□), 10 sccm (0), 50 sccm (Δ), 75 sccm (□), 100 sccm (∇), 150 sccm (x).

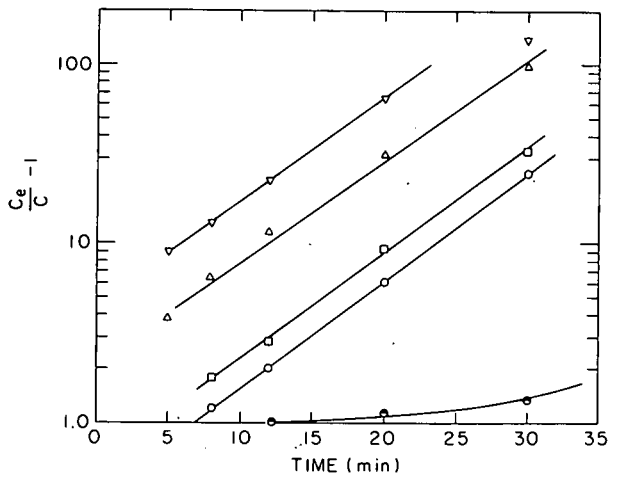

Figure 6. Plots of log (C_e/C - 1) versus time; 150 sccm (∇), 100 sccm (▽), 75 sccm (□), 50 sccm (0), 10 sccm (θ).

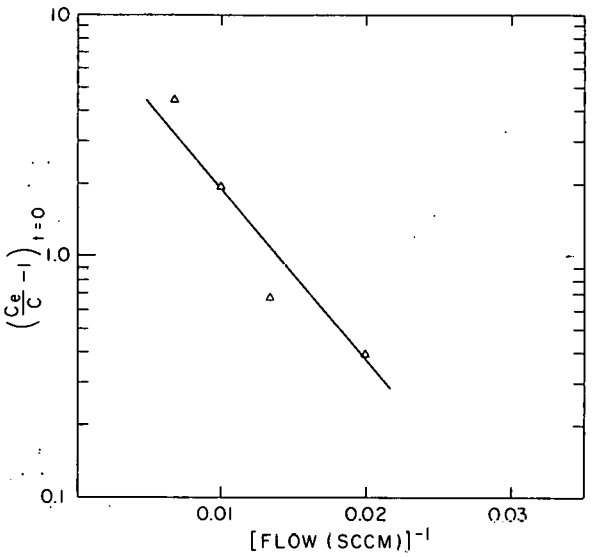

Figure 7. Plot of log $(C_e/C - 1)_{t=0}$ versus reciprocal flow rates.

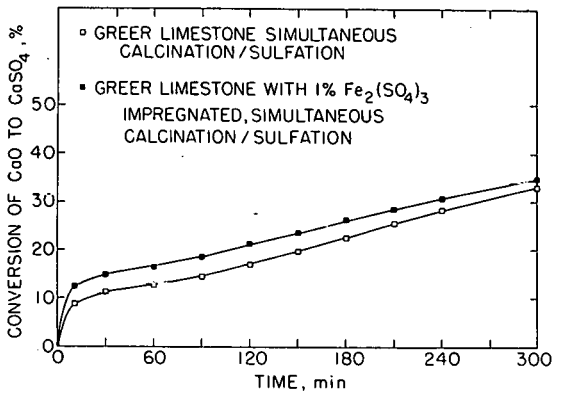

Figure 8. Enchancement of Greer limestone sulfation with 1% $Fe_2(SO_4)_3$ impregnated, simultaneous calcination/ sulfation at 900°C in 0.25% SO_2, 5% O_2, 17% CO_2, 5% H_2O and a balance of N_2.

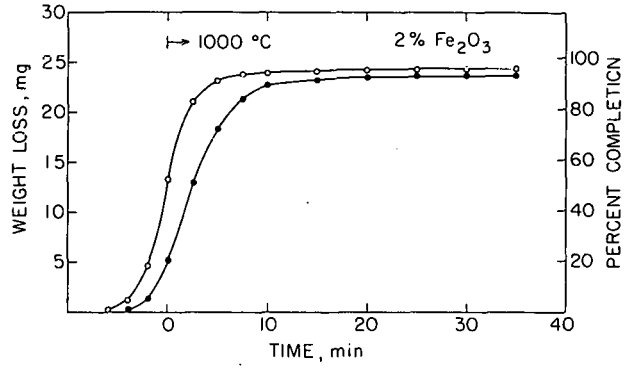

Figure 9. Rate of reaction $3CaSO_4 + CaS \rightarrow 4CaO + 4SO_2$ at 1000°C in N_2 with powdered reagent grade samples.

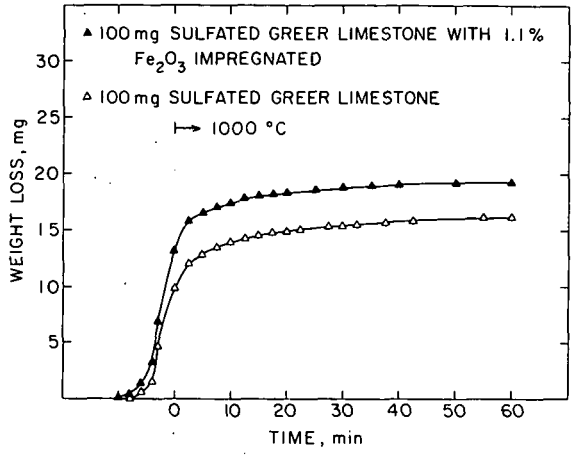

Figure 10. Rate of regeneration $CaSO_4 + 1/2C \rightarrow CaO + 1/2CO_2 + SO_2$ at 1000°C, with 100 mg 20.7% sulfated Greer limestone (16/20 mesh) and fly ash (ANL LST-7B) containing 8.55% carbon.

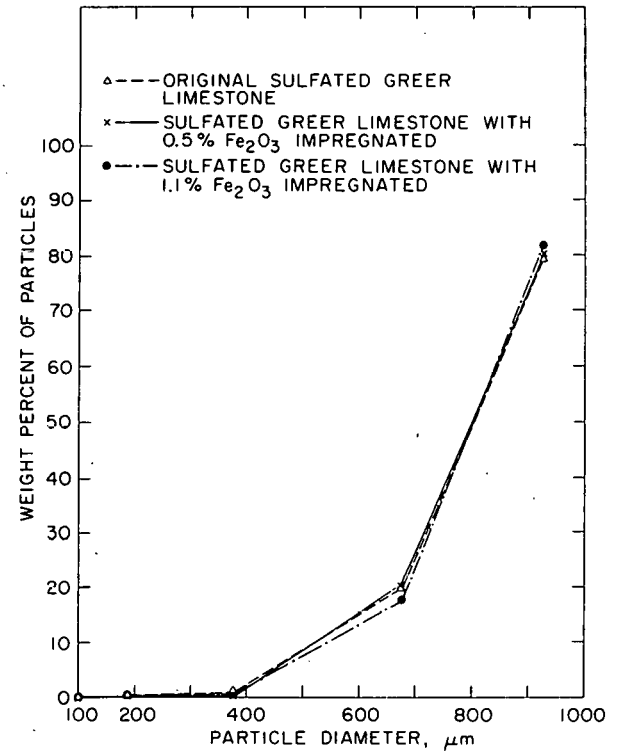

Figure 11. Particle size distributions of the sulfated Greer limestone with and without iron oxide coated after 5 hours of sulfation at 900°C in a fluidized-bed sulfator.

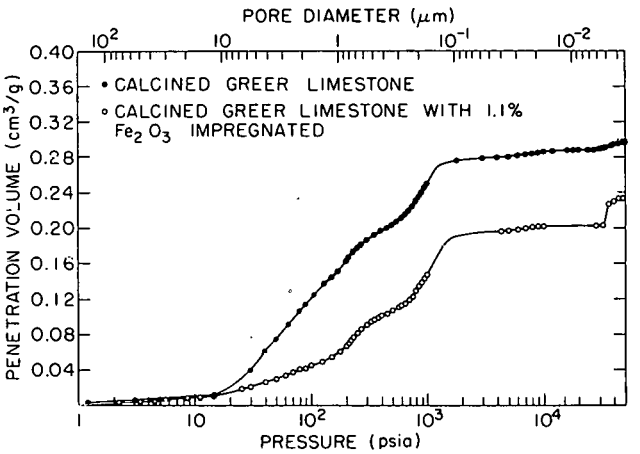

Figure 12. Porosimetry curves for the Greer limestone with and without iron oxide coated, calcined 1 hour at 900°C in N_2.

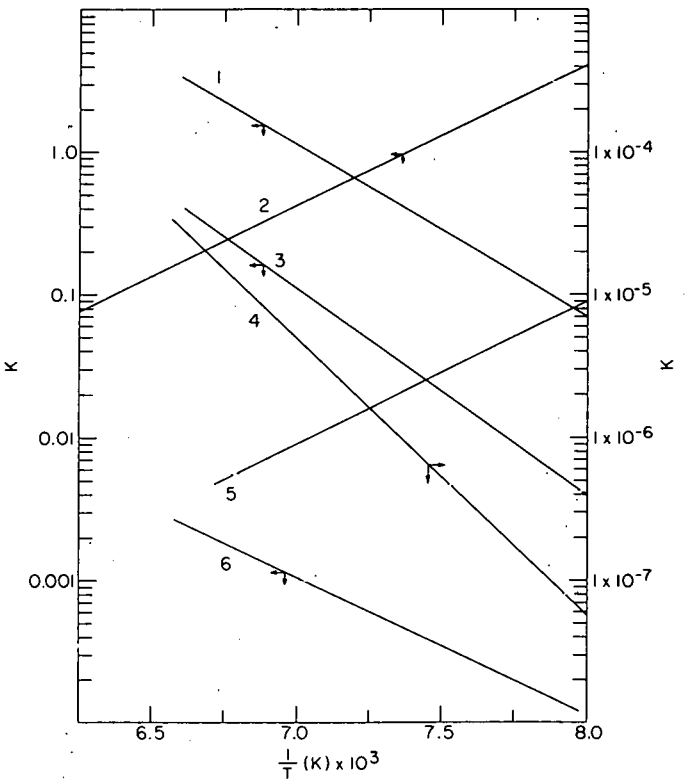

Figure 13. 1) $1/4CaS + 3/4CaSO_4 \rightarrow CaO + SO_2$
2) $2/3CaO + SO_2 \rightarrow 2/3CaSO_4 + 1/6S_2$
3) $3/2CaS + 1/2CaSO_4 \rightarrow 2CaO + S_2$
4) $CaSO_4 \rightarrow 2CaO + SO_3$
5) $CaS + 2SO_2 \rightarrow CaSO_4 + S_2$
6) $2CaS + SO_2 \rightarrow 2CaO + 3/2S_2$

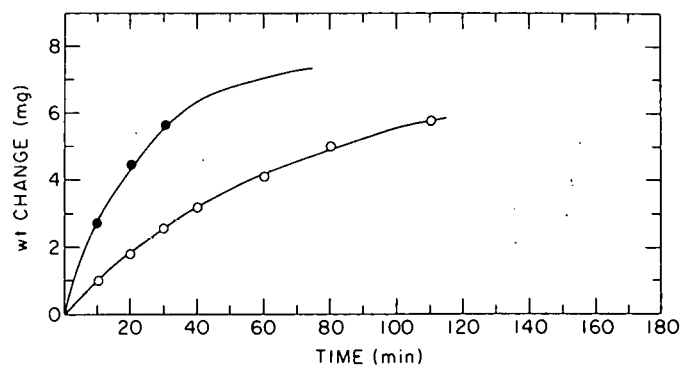

Figure 14. Reactions of CaS (21 mg), with SO_2 (8%) and CaS (2.1 mg) with O_2 (10%) at 1000°C; with O_2 (●), with SO_2 (○).

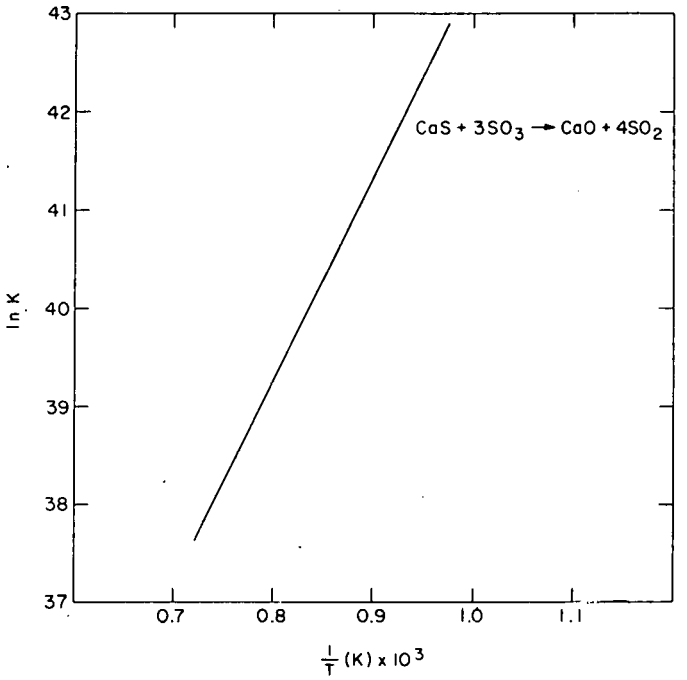

Figure 15. Equilibrium constants versus reciprocol temperature for CaS with SO_3.

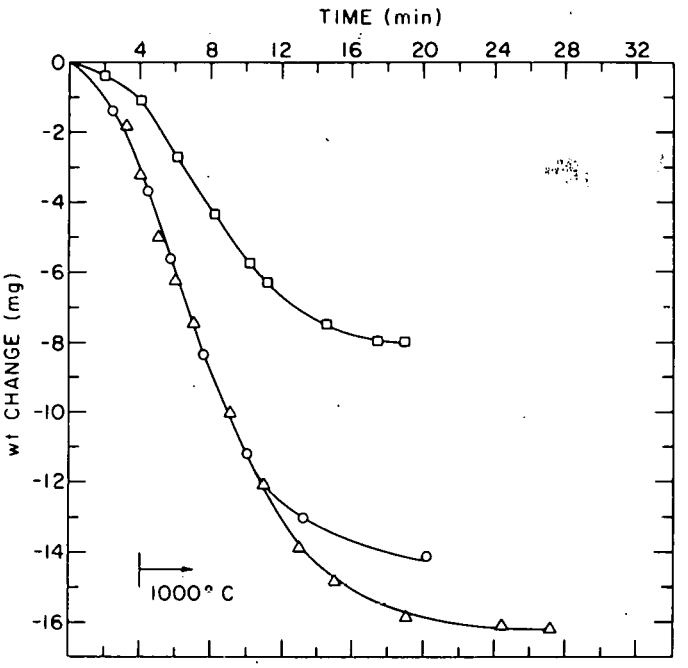

Figure 16. Wt changes versus time for CaS with $CaSO_4$ reaction at 1000°C; CaS (9.6 mg) + $CaSO_4$ (27 mg) (Δ), CaS (4.8 mg) + $CaSO_4$ (27 mg) (0), CaS (10 mg) + $CaSO_4$ (14 mg) (□).

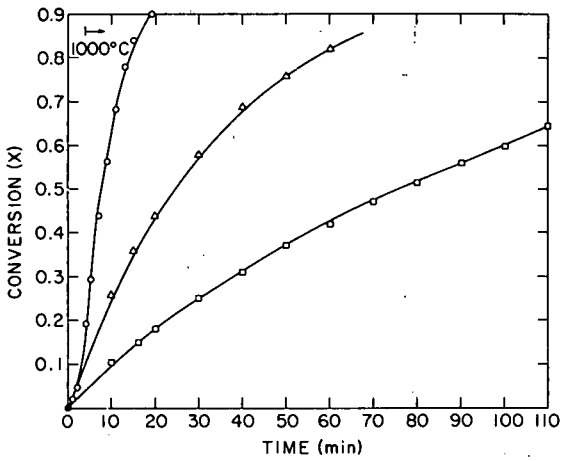

Figure 17. Reaction rates of $3CaSO_4 + CaS \rightarrow 4CaO + 4SO_2$; T = 1000°C (0), 950°C (Δ), 900°C ( ).

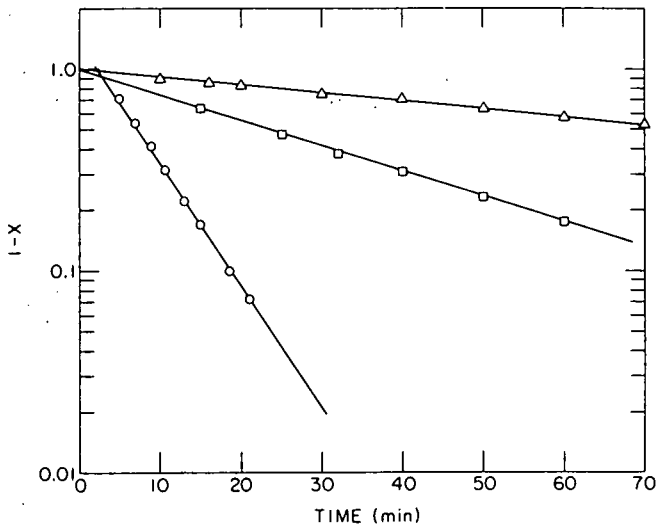

Figure 18. First order rate correlation for CaS with $CaSO_4$ reaction; T = 1000°C (0), 950°C ( ), 900°C (Δ).

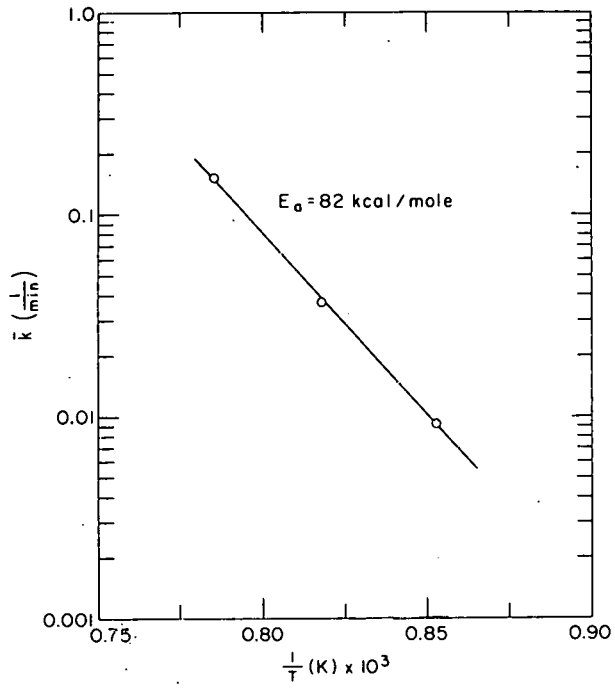

Figure 19. Temperature dependence of rate constant, $\bar{k}$, for CaS with $CaSO_4$ reaction.

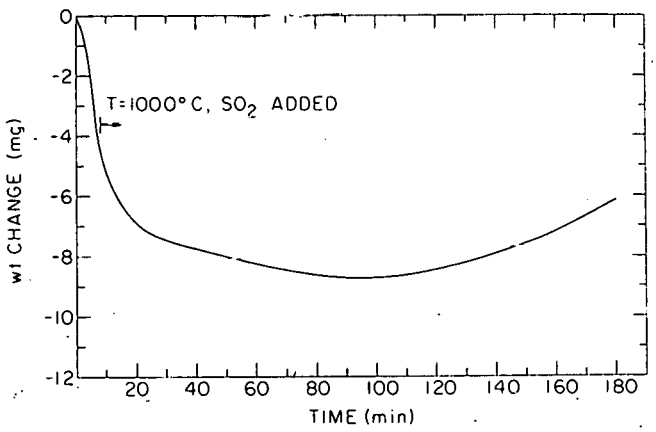

Figure 20. Wt changes of $CaSO_4$ (27 mg) with CaS (9 mg) versus time under SO_2 (4%) at 1000°C.

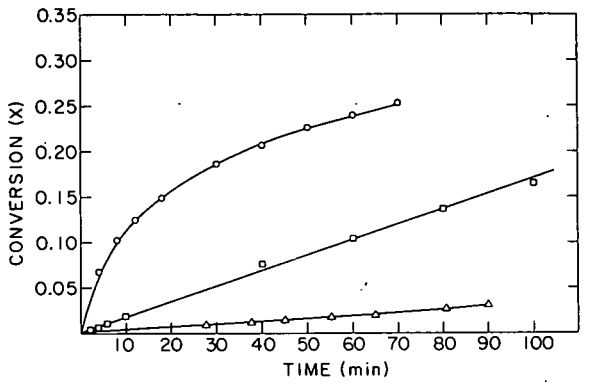

Figure 21. Reaction rates of CaO with SO_2 (4%); T = 950°C (0), 1000°C ( ), 1100°C (Δ).

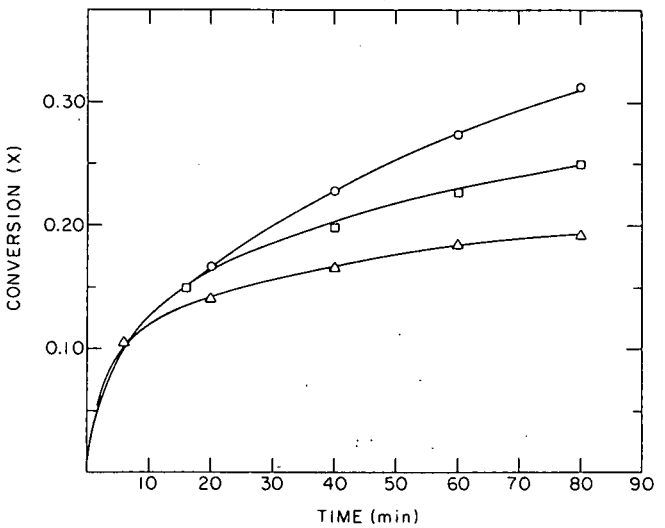

Figure 22. CaS with SO_2 reaction rates; T = 1000°C (0), 950°C (□), 900°C (Δ).

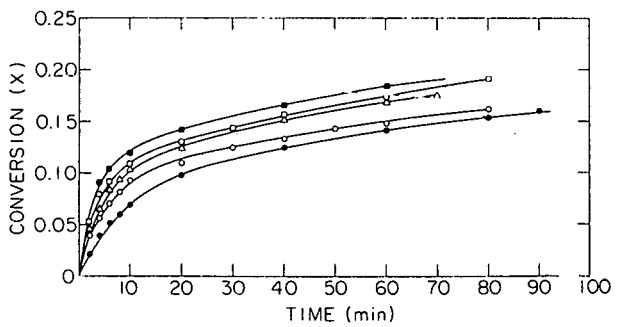

Figure 23. CaS with SO_2 reaction rates at 900°C; SO_2 composition = 16% (□), 11% (■), 8% (Δ), 6% (0), 4% (0).

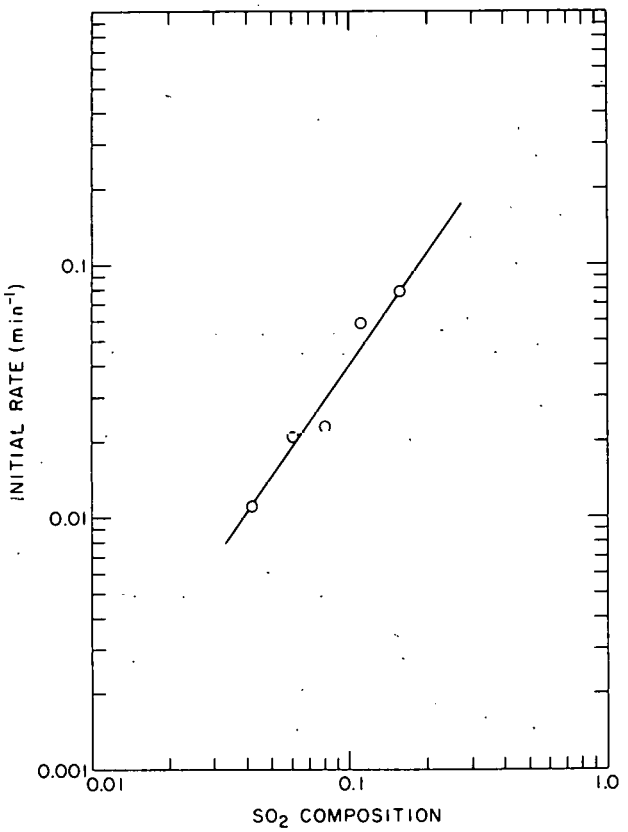

Figure 24. Rate dependence of CaS with SO_2 reaction on SO_2 concentration at 900°C.

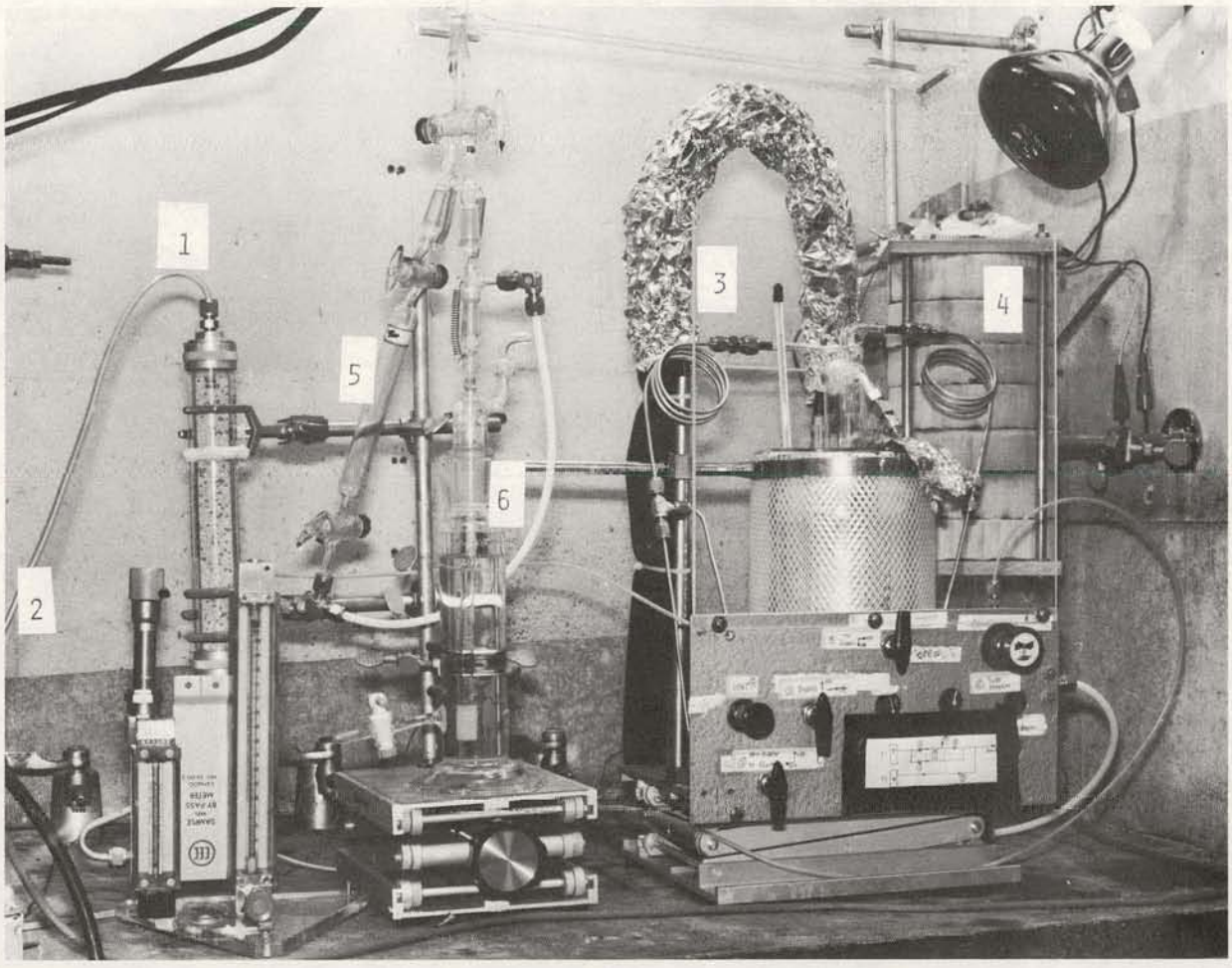

Figure 25. Apparatus for CaO with SO_3 reaction measurements. (1) drier, (2) rotameters, (3) SO_3 scrubber, (4) reactor, (5) sampling bulb, and (6) scrubber.

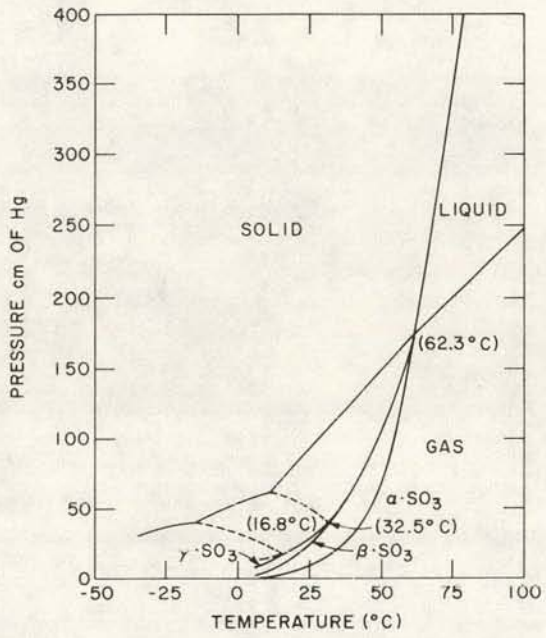

Figure 26. Vapor pressure relations for modifications of sulfur oxide.

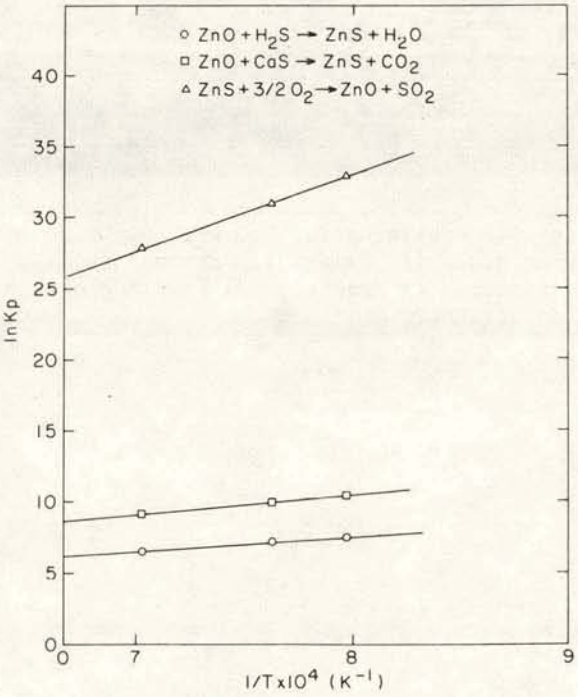

Figure 27. Equilibrium constants.

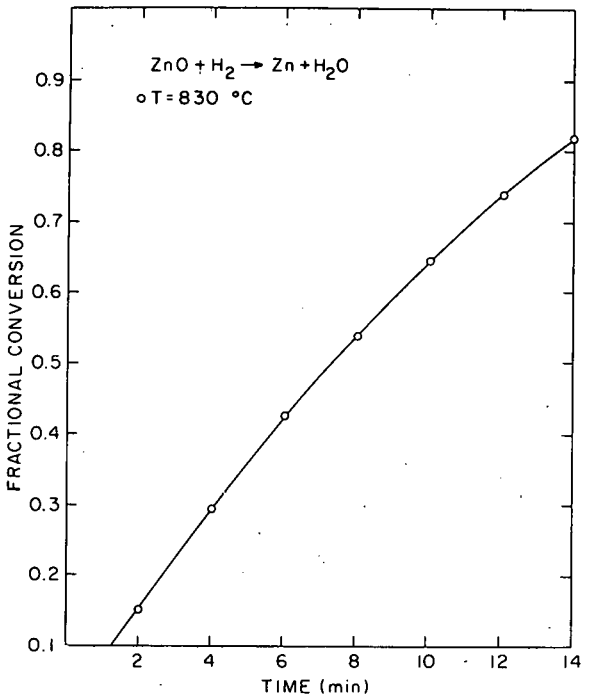

Figure 28. Heats of reaction.

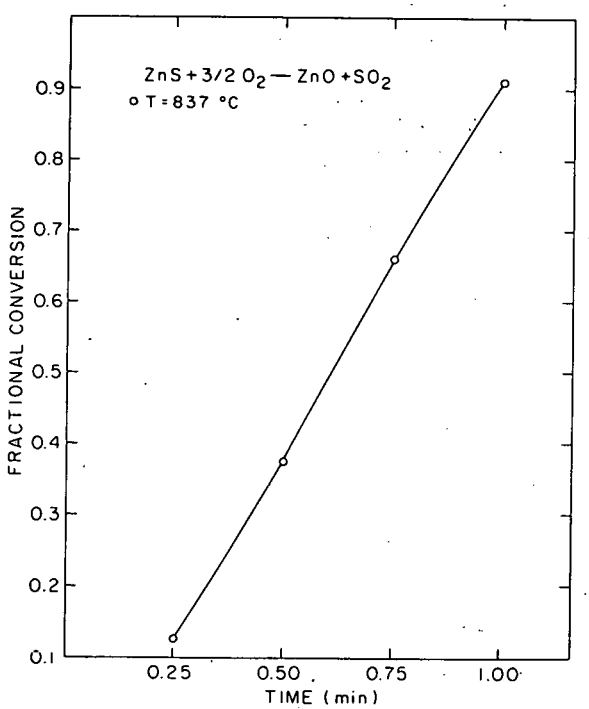

Figure 29. Rate of sulfidation.

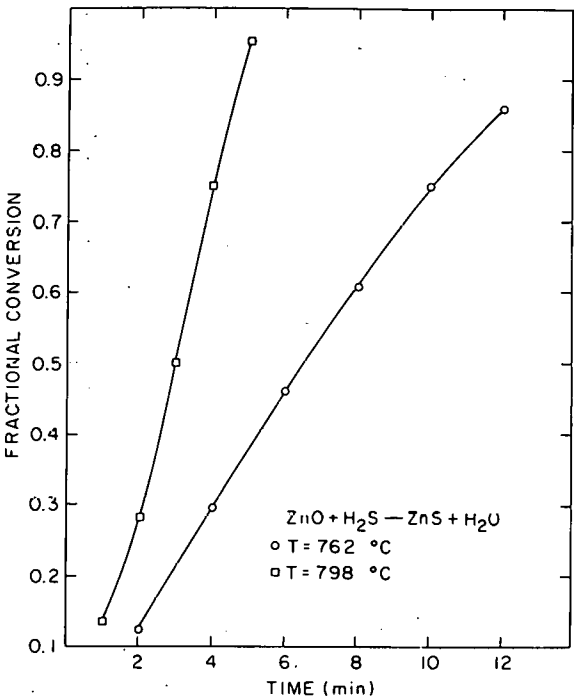

Figure 30. Rate of oxidation.

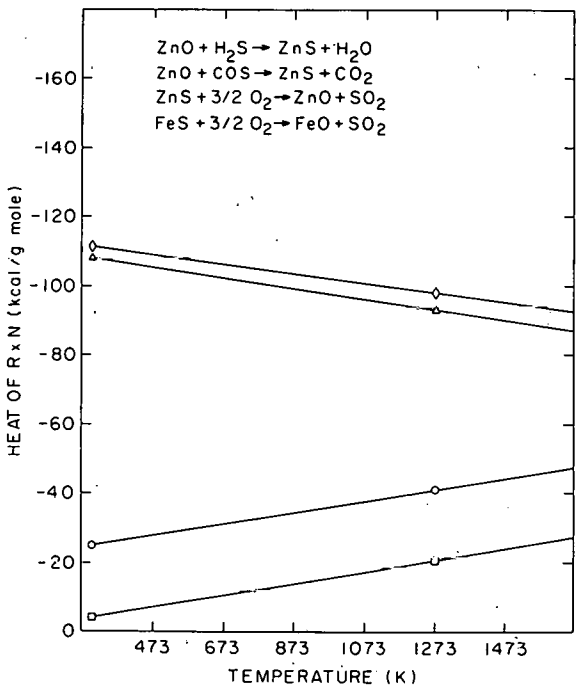

Figure 31. Rate of evaporation of ZnO in reducing atmosphere.

Distribution:

W. Fedarko, FE/DOE (10)
A. Macek, FE/DOE
W. E. Winsche, BNL
K. C. Hoffman, BNL
B. Manowitz, BNL
D. Gurinsky, BNL
M. Steinberg, BNL
R. T. Yang, BNL
N. Abauf, BNL
A. S. Albanese, BNL
J. M. Chen, BNL
G. Farber, BNL
F. B. Kainz, BNL
C. R. Krishna, BNL
J. Pruzansky, BNL
M-S. Shen, BNL
R. H. Whisker, BNL
D. Schweller, DOE (BNL)
R. Smol, BNL
D. B. Henschel, EPA
J. W. Jones, EPA
F. Princiotta, EPA
H. B. Levine, Jaycor
F. B. Hill, BNL
C. H. Waide, BNL
C. L. Steen, BNL
D. M. Roy, PSU
K. S. Horr, Fiberboard